Wall Elasticity Effects on Carotid Hemodynamics and LDL Mass Transport; a Computational Approach

Shahab Khakpour[1], Azadeh Shahidian[2,*] and Majid Ghassemi[2]

[1]*Research Unit of Medical Imaging, Physics and Technology, Faculty of Medicine, University of Oulu, Finland*

[2]*Mechanical Engineering Department, K. N. Toosi University of Technology, Tehran, Iran*

Abstract: Cardiovascular diseases takes many lives yearly, whereas atherosclerosis is on the top. Carotid atherosclerosis disease considered as a multi-aspects disease and only by considering all of its aspects, a comprehensive insight can be achieved. It seems that wall motion has great effects on arterial hemodynamics and Low Density Lipoprotein (LDL)mass transport and concentration while LDL concentration is believed to be highly associated with atherosclerosis plaque formation. The primary goal of this study is to investigate the wall elasticity effects on carotid hemodynamics and LDL mass transport through carotid artery bifurcation as a challenging case due to its geometry and location. The blood is modeled as Carreau fluid which is considered as a well-behavior model for blood. A pulsatile speed profile applied as the inlet boundary and two-ways Fluid Structure Interaction (FSI) transient analysis is performed to achieve more accurate. In order to investigate wall elasticity effects, the carotid bifurcation modeled as solid, linear elastic and hyperelastic (Mooney-Rivlin). As the high LDL concentration can be considered as atherogenes is region indicator, therefore, it is used as the criterion for assessing the different arterial wall assumption. The wall elasticity effects on the hemodynamics are presented in three-time steps; early systole, end systole and end diastole. Results show that linear elastic and hyperelastic models predict very alike flow pattern however wall deformation and behavior are totally different. Results indicatet hat solid wall assumption is not appropriate for large and complicated arteries such as carotid bifurcation. Hyperelastic model (Mooney-Rivlin) seems more relevant and one the second place, the linear wall elastic model may be a good choice.

Keywords: Wall elasticity, Blood Flow, LDL, FSI analysis, Atherosclerosis and Carotid artery.

1. INTRODUCTION

During recent years, due to full fat diets, smoking, hypertension and some other risk factors, cardiovascular disease especially atherosclerosis has taken many lives in modern countries [1]. Atherosclerosis plaques mostly take form in locations which flow deviates from its general pattern (such as aorta, coronary and carotid sinus). In these areas shear stress is low, LDL mass ratio is high, and flow separation and recirculation zones may be observed. In many numerical researches such as Perk told [2] Marshall *et al*, [3] and the experimental works like [4] arterial wall motion is ignored and wall assumed to be solid.

Because of the wall elasticity plays major role in converting pulsatile flow to more uniform flow, it seems that solid wall model is not suitable for large arteries like aorta and carotid.

Moayeri [5] and Zhao *et al*, [6] are used linear elasticity in their works. Some papers like Stephan is [7] investigate the wall elasticity module and report different values by different methods. The arterial wall has a multi-layer structure and when it stretches, it will become stiffer, so carotid bifurcation behavior is similar to hyperelastic materials. One of the best hyperelastic models is Mooney-Rivlin. Valencia [8] and Mehmet *et al*, [9] use this model in their works. Blood modeled as Newtonian [6] and non-Newtonian fluid [10] but is accepted that if blood shear rate is more than 100(1/s), blood behaves like a Newtonian fluid. In large arteries in vicinity of the heart, due to high velocity, shear rate is high and red blood cells move in parallel manner. In this state, many researchers [6, 11] assumed that blood is a Newtonian fluid but in arteries with more complicated geometry like carotid bifurcation, flow separation and recirculation may occur and therefore shear rate becomes very low and we should not use a Newtonian blood model. Many Non-Newtonian models like Casson [12], Carreau [13], Carreau-Yassuda [14] and power law models [14] are presented for blood mimicking fluid. Among stall these models, Carreau model seems to be the best choice. Often the out of-plane curvature of the ICA ignored in average models [2, 3]. There is variant 2D [12, 15] and 3D [10, 16] carotid models. In 2D model secondary flow cannot be seen. The 3D geometrical models divided in two categories; the average model [15] and the realistic model [16].

Due to some arteries complicated geometry (such as carotid) the flow deviates from its main pattern. So these arteries become potential to atherosclerosis. As a result, low density lipoprotein (LDL) concentration

*Address correspondence to these authors at the Mechanical Engineering Department, K. N. Toosi University of Technology, Tehran, Iran;
Tel: +989124193914; +982184063287; Fax: +982188674748;
E-mail: shahidian@kntu.ac.ir; az_shahidian@yahoo.com

E-ISSN: 2311-8792/17

increases and infiltrates the endothelial layer (especially in hypertension) which leads to athero-sclerosis plaque formation [17]. It is believed that after infiltration, LDL molecules are oxidized and this causes a chain of chemical interactions, which result plaque formation factors to be absorbed [18,19,20]. Because of plaque formation and consequently artery lumen reduction, thrombosis is more likely to be trapped. Also artery may be occluded or plaque may be ruptured and may consequently cause plaque bleeding, recovering and re-growing [17]. It assumed that infiltration is higher in places with high LDL concentration. LDL concentration increases in regions which are associated with low shear stress, flow separation and recirculation [18, 19]. So LDL concentration is a good sign for plaque formation. Because of wall elasticity role in flow properties and LDL concentration, investigating wall elasticity effects on blood flow domain and LDL mass transfer through carotid bifurcation are the current study purposes.

In this study, three wall models have been used: 1) solid wall, 2) linear elastic and 3) Mooney-Rivlin (hyperelastic material). The Carreau model is used for blood simulation. Also Fluid Structure Interaction (FSI) analysis in elastic cases is performed to obtain more realistic results.

2. PROPOSED MODEL

The schematic of the 3D averaged model of the carotid bifurcation is depicted in Figure **1**. The geometrical model is structured according to the Bharadvaj (1982) [21].

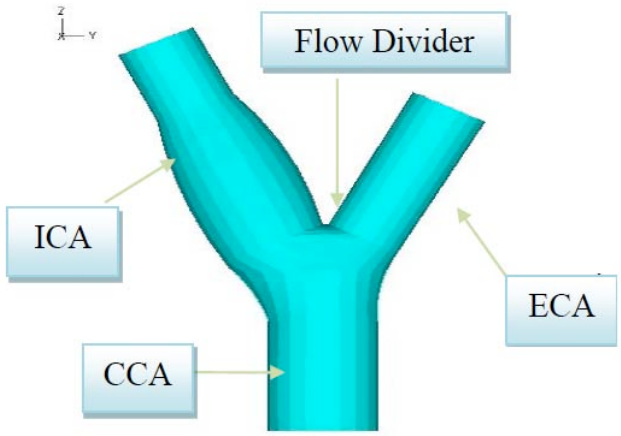

Figure 1: Averaged model of carotid bifurcation.

As shown Common Carotid Artery (CCA), Internal Carotid Artery (ICA) and External Carotid Artery (ECA) are coplanar and the flow divider is assumed as a blunt nose. All cross section considered to be circular.

Figure **2** is shown the schematic of the 3D model of the blood.

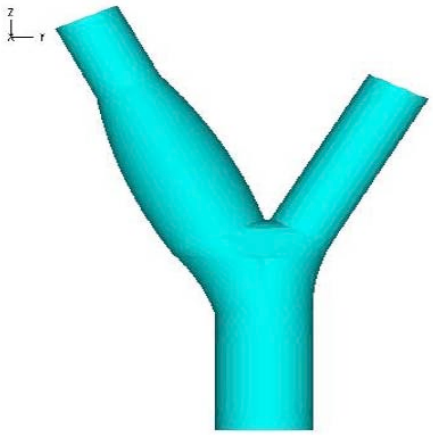

Figure 2: Blood model.

3. GOVERNING EQUATIONS

The continuity, Navier-Stocks and mass transfer equations in 3D transient incompressible flow are used as follows:

Continuity equation:

$$\nabla.(\vec{V})=0 \quad (1)$$

Navier-Stocks equation:

$$\rho\left(\frac{\partial\vec{V}}{\partial t}+\vec{V}.\nabla\vec{V}\right)=-\nabla p+\nabla T+\rho F \quad (2)$$

Mass transfer equation:

$$\frac{\partial\rho\emptyset_{LDL}}{\partial t}+\nabla.\left(\rho\vec{V}\emptyset_{LDL}-\rho D_{LDL}.\nabla\emptyset_{LDL}\right)=m''' \quad (3)$$

Where $\vec{V},p,T,\rho,F$ and D_{LDL} are velocity field, pressure, stress tensor, bulk density, body force, and LDL diffusion coefficient in blood respectively. LDL mass ratio ($\emptyset_{LDL}$) is equal to $\frac{\rho_{LDL}}{\rho}$. Also m^m is mass creation rate. Bulk density was considered 1060 $^{Kg}/_{m^3}$[22]. At 37°C, LDL diffusion coefficient in blood (D_{LDL}) is equal to $2\times10^{-13}\ ^{m^2}/_{s}$ [23].

3.1. Blood

Blood consists of Blood Cells and plasma [22]. The upper limit and the lower limit of blood viscosity are 0.056pa.s and 0.00345pa.s respectively [24]. The Carreau model is used to simulate blood viscosity in

stress tensor of Navier Stocks equation. The Carreau viscosity equation is as follow:

$$\mu_{eff} = \mu_{\infty} + (\mu_0 - \mu_{\infty})(1 + A\dot{\gamma}^{2})^{n} \quad (4)$$

Where A, μ_0, μ_{∞} and n are constant, $\dot{\gamma}$ is effective deformation rate and μ_{eff} is effective viscosity. For blood μ_{∞},μ_0, A andnare 0.00345Pa.s, 0.056Pa.s, 10.976 and -0.3216 respectively [14].

3.2. Arterial Walls

In this research, wall modeled as solid, linear elastic and hyperelastic. In case of solid model, only blood model can be used. In linear elastic model, stress-strain relationship defines as below:

$$\sigma = E\varepsilon \quad (5)$$

Where σ, E and ε are stress tensor, linear elasticity module and strain tensor.

In fact, the artery wall behaves as a hyperelastic material. The Mooney-Rivlin model is one of the best hyperelastic material models that express relation between strain energy and strain invariant. This strain energy function is given by:

$$W_D = C_1(I_1 - 3) + C_2(I_2 - 3) + C_3(I_1 - 3)^2 + C_4(I_1 - 3)(I_2 - 3) + C_5(I_2 - 3)^2 + C_6(I_1 - 3)^3 + C_7(I_1 - 3)^2(I_2 - 3) + C_8(I_1 - 3)(I_2 - 3)^2 + C_9(I_2 - 3)^3 + D_1(Exp(D_2(I_1 - 3)) - 1 \quad (6)$$

Where W_D and I_i are strain energy density and strain invariant respectively. For arterial wall, C_i (i=1 to 9), D_1 and D_2 are 0,2613.4Pa and 8.5 [25].

Arterial wall thickness is between 0.08-0.1 artery lumen [6]. In this study arterial wall thickness has been considered 0.1.

Also Fluid Structure Interaction (FSI) analysis in linear elastic and hyper elastic models is performed. In fluid-structure interaction analyses, fluid forces are applied onto the solid and the solid deformation changes the fluid domain. The interaction occurs along the interface of the solid and fluid domains. The FSI analysis represents the most accurate results in large arteries like carotid bifurcation [10, 26].

4. BOUNDARY AND INITIAL CONDITIONS

The initial conditions are assumed as follow:

$$V_x = 0, V_y = 0\, V_z = 0.0705\ {}^{m}/_{s}$$

These values are equal to the last CCA inlet velocity, in a cardiac cycle.

Also,

$\emptyset_{LDL}$ =0, m^m=0 at walls.

The boundary conditions are assumed as follow:

ICA outlet: Free boundary condition

ECA outlet: Free boundary condition

CCA inlet: $\emptyset_{LDL}$=1 and pulsatile velocity (Figure **3**).

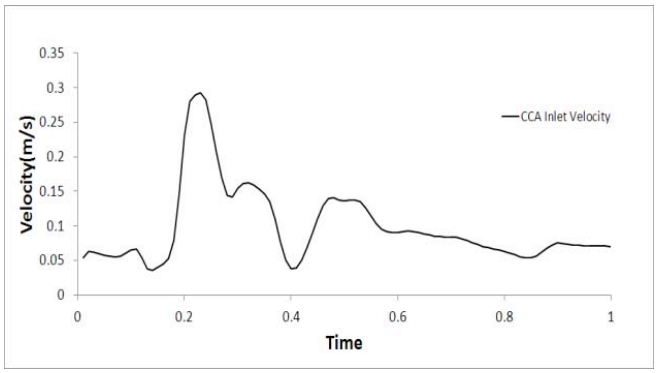

Figure 3: Velocity wave in CCA inlet B.C [14].

As shown in figure **3**, blood flow in CCA inlet is completely pulsatile [2].

Reynolds number: Re= 118 to 728 (based on the common carotid artery entrance).

5. NUMERICAL SCHEME

In this study a commercial software package based on finite element method (ADINA) is used. An unstructured mesh and structured mesh are used for the blood and the artery wall respectively. A coarse mesh applied and 26 times refined until mesh size independency achieved. Figure **4** is shown the grid study.

Finally, the 180113FCBI-C(fluid Flow Condition Based Interpolation) elements (720452 nodes) and the 3500 solid elements (28000 nodes) are used. After 2 cycles, the relative fluid and mass transfer variables error was less than 2 percent; so all results is presented from second to third cycle.

The applied method for FSI analysis is iterative and three 2.4Giga Hz processors with 4Giga bytes RAM within three days are used to obtain 3-cycle converged solution.

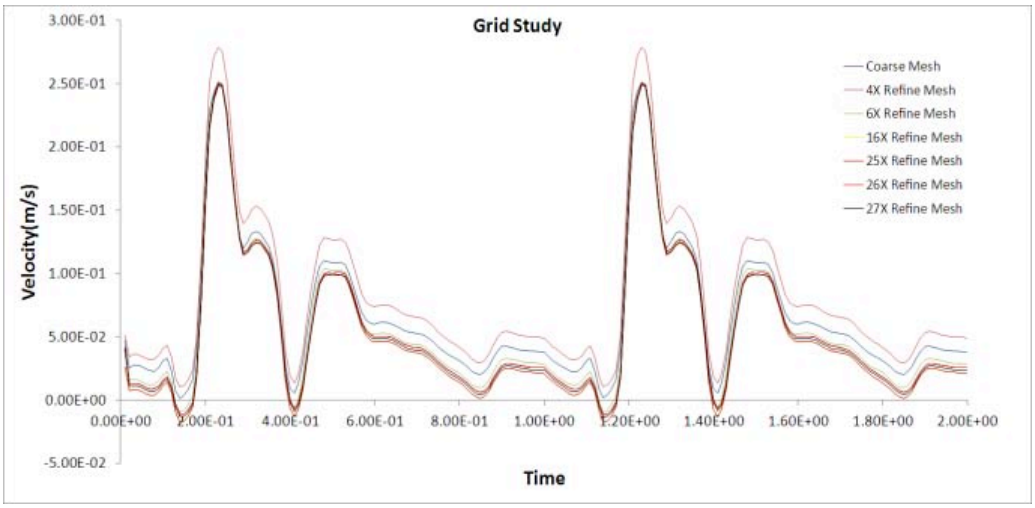

Figure 4: Grid study (axial velocity, CCA middle).

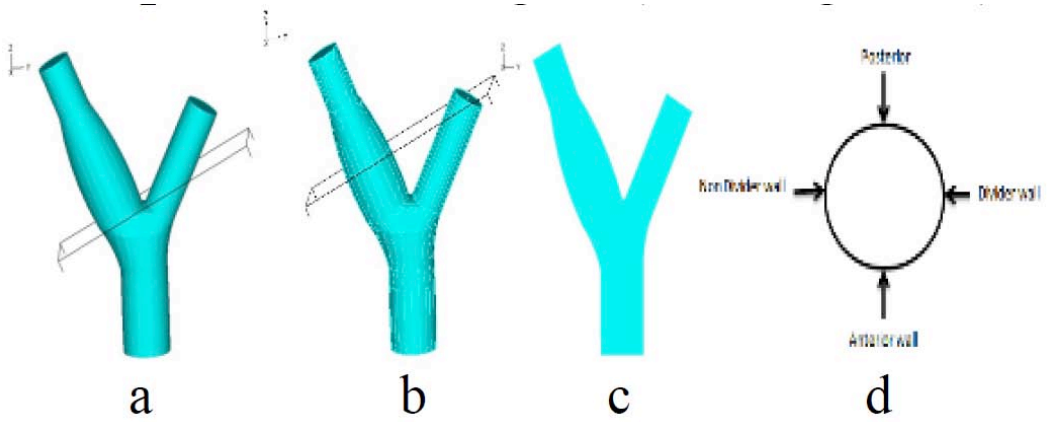

Figure 5: Cross sections: (**a**) ICA inlet (**b**) ICA sinus (**c**) axial plane (**d**) Walls positions.

6. RESULTS

The propose of this study is to investigate wall elasticity effects on flow domain and LDL mass transfer inside of carotid bifurcation. To investigate the flow phenomena in carotid bifurcation, three cross sections were selected: one cross section at the inlet, one cross section at sinus region of internal carotid artery and the other cross section selected at axial plane of common carotid artery for better flow phenomena sight. (See Figure **5**)

Velocity vector plot and LDL Mass Ratio (MR) band plot in three non-dimensional times are shown in results. These non-dimensional times are early systole (t/t_p =0.2), end systole (t/t_p =0.35) and end diastole (t/t_p=0.9)) of a cardiac cycle time (t_p). In many researches such as Sui *et al,* [27], low WSS introduced as an important factor of atherosclerosis plaque formation. So wall shear stress (WSS) components at sinus region are plotted.

6.1. Velocity Vectors

In this section, velocity vector plots for better understanding of flow phenomena like vortexes and flow direction are presented.

The velocity profile at the entrance of internal carotid and early systole is shown in figure **6**. In Mooney-Rivlin and linear elastic models, flow moves from non-divider wall (through the anterior and posterior walls) toward divider wall but in solid model, flow is weaker than the two other models. In solid model, the flow uniformly moves from non-divider wall towards divider wall.

As shown in figure **7**, the Mooney-Rivlin and the linear elastic models predict similar flow patterns at the entrance of internal carotid at end systole. In these models, flow moves from non-divider wall toward divider wall through posterior wall. Also two vortexes can be observed; one clock wise (CW) vortex at anterior side of divider wall and the other a contra clock

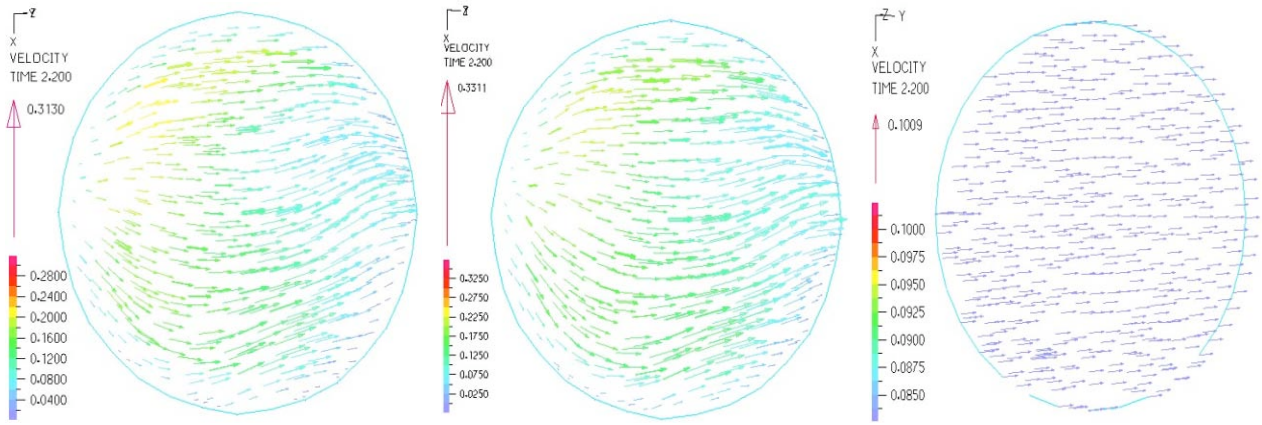

Figure 6: Velocity vector plot at ICA entrance and early systole (t/t_p=2.2). From left to right: Mooney-Rivlin, linear elastic and solid models.

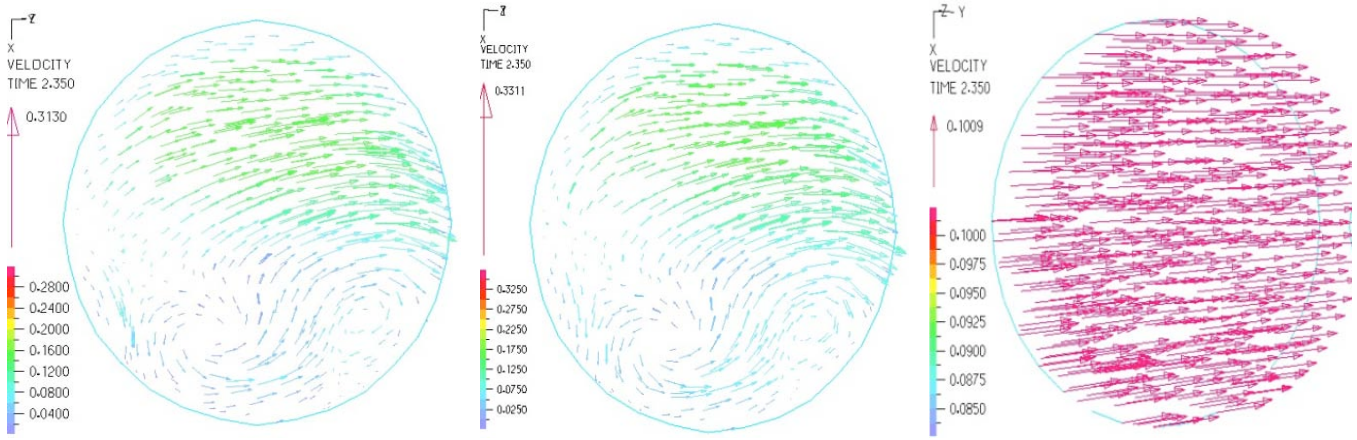

Figure 7: Velocity vector plot at ICA entrance and end systole (t/t_p=2.35). From left to right: Mooney-Rivlin, linear elastic and solid models.

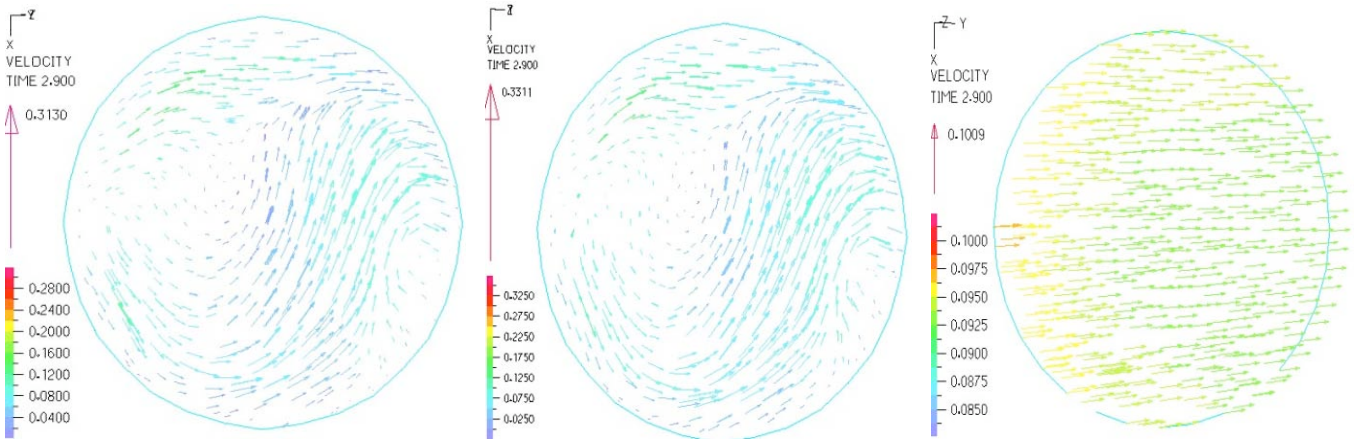

Figure 8: Velocity vector plot at ICA entrance and end diastole (t/t_p=2.90). From left to right: Mooney-Rivlin, linear elastic and solid models.

wise (CCW) vortex at anterior side of non-divider wall. The solid wall model predicts low magnitude and highly unidirectional flow from non-divider wall to divider wall.

As shown in figure **8**, the Moon-Rivlin and the linear elastic models, two large vortexes occupy the most part of the cross section at the entrance of internal carotid at end diastole. The bigger vortex (CCW) locates at non-divider wall and center regions and smaller one (CW) can be seen at anterior side of divider wall. Again in the solid model flow is weaker and its direction is from non-divider wall toward divider wall.

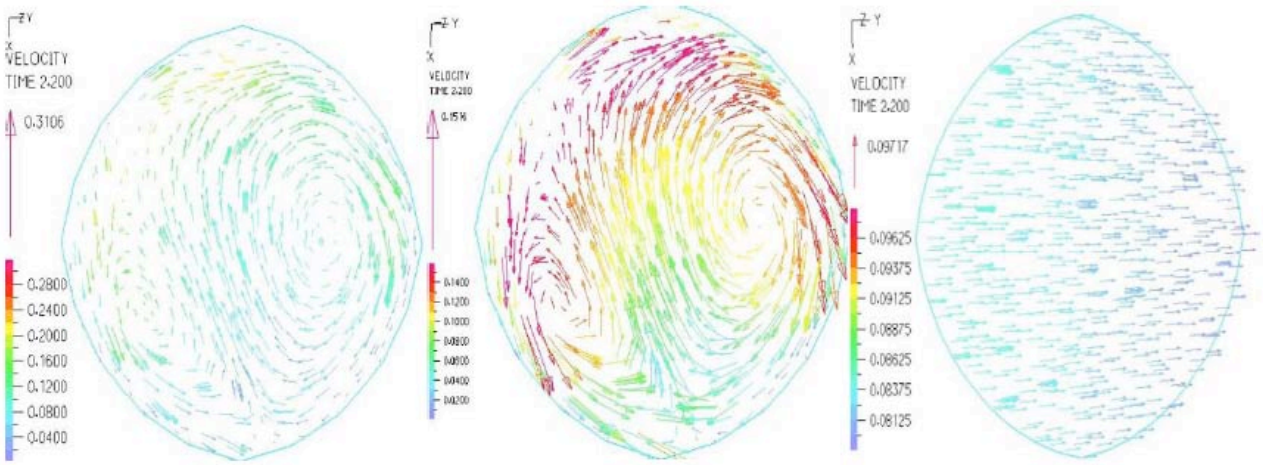

Figure 9: Velocity vector plot at ICAsinus and early systole (t/t_p=2.2). From left to right: Mooney-Rivlin, linear elastic and solid models.

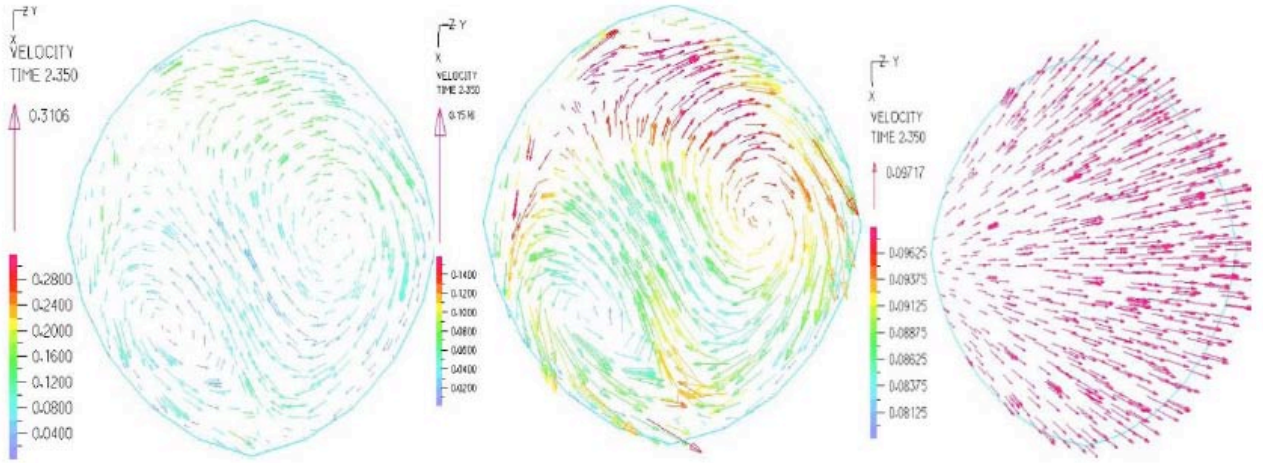

Figure10: Velocity vector plot at ICAsinus and end systole (t/t_p=2.35). From left to right: Mooney-Rivlin, linear elastic and solid models.

The velocity profile at sinus region and early systole is shown in figure **9**. In the Mooney-Rivlin and linear elastic models, divider wall vortex (CW) is very larger than non-divider wall vortex (CCW) and approximately occupies 60% of the cross section. Non divider wall vortex is highly stretched and locates on the anterior side of non-divider wall. The velocity magnitude in Mooney-Rivlin model is higher than linear elastic model. Again, solid wall model predicts lower velocity magnitude and high unidirectional flow from non-divider wall to divider wall.

The velocity pattern at the sinus region and end systole is similar to early systole results for the Mooney-Rivlin and linear elastic models. But in solid model, blood moves from non-divider wall and flows toward other three walls. These results are shown in figure **10**.

The velocity profile at sinus region and end diastole is shown in figure **11**. In the linear elastic and the Mooney-Rivlin models, two vortexes are very similar to their end systole status results but are more stretched. In solid model, the flow direction from non-divider toward divider wall is fixed and no vortexes can be observed.

Figure **12** is shown the velocity profile at axial cutting plane and early systole. As shown in the elastic and Mooney-Rivlin models, flow mostly transfers from CCA in vicinity of non-divider wall to ICA and accelerates at ICA outlet. In Mooney-Rivlin model, flow in ECA skewed towards divider wall but in linear elastic model high value velocity occupies entire of ECA. Also Mooney-Rivlin model predicts higher velocity values than linear elastic model. In solid model flow is very uniform and moves parallel to CCA axis and moves like a wave.

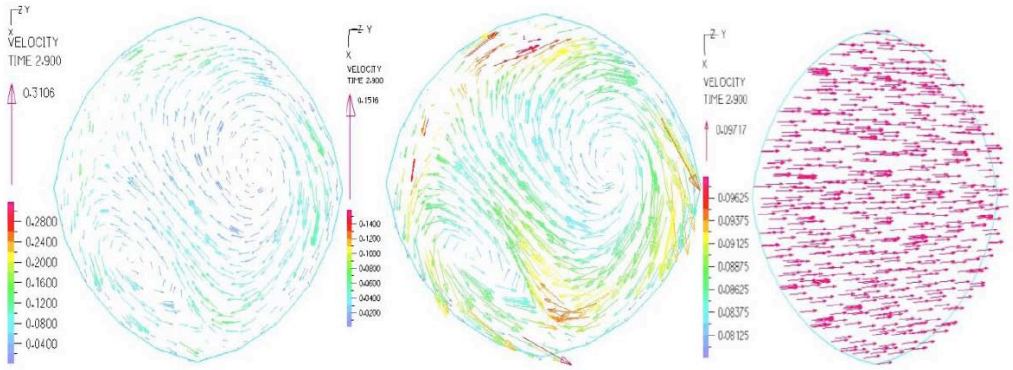

Figure11: Velocity vector plot at ICAsinus and end diastole (t/t_p=2.90). From left to right: Mooney-Rivlin, linear elastic and solid models.

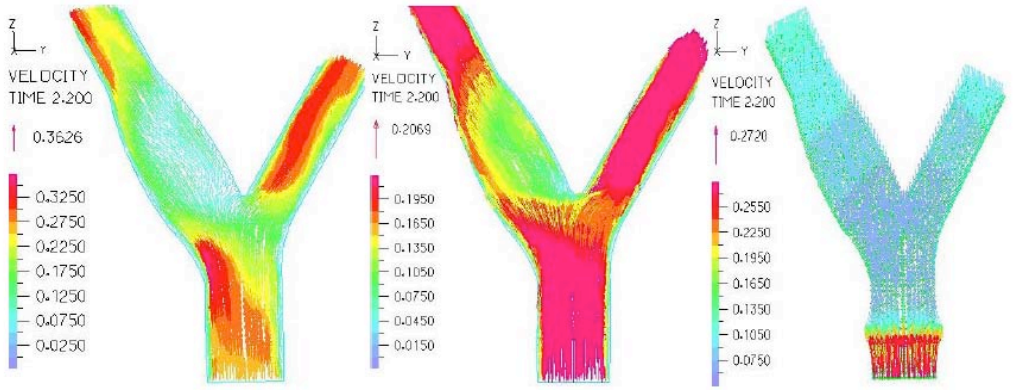

Figure12: Velocity vector plot at axial plane and early systole(t/t_p=2.2). From left to right: Mooney-Rivlin, linear elastic and solid models.

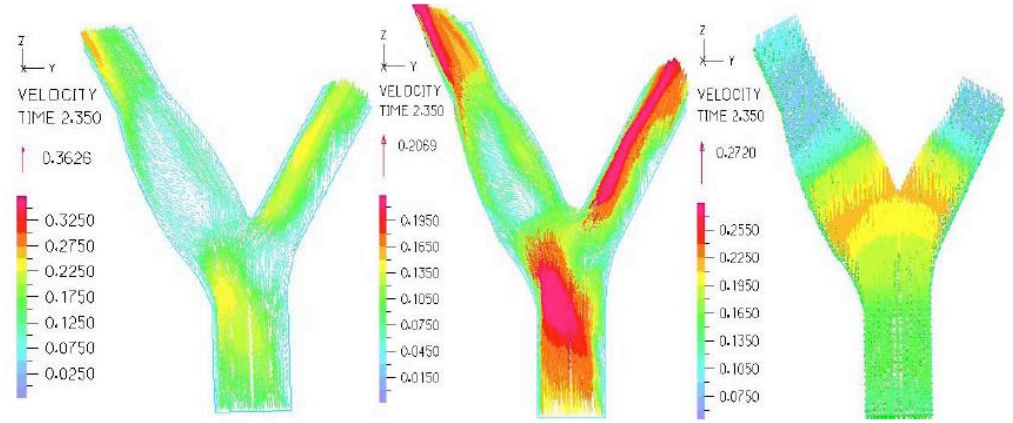

Figure13: Velocity vector plot at axial plane and end systole(t/t_p=2.35). From left to right: Mooney-Rivlin, linear elastic and solid models.

Figure **13** is shown the velocity profile at axial cutting plane and end systole. Results show that in Mooney-Rivlin model, the flow concentrates in center regions of CCA and a big vortex occupies the most part of ICA sinus in Mooney-Rivlin model. Also a separation zone can be seen at non-divider wall of ICA entrance. In this model, Flow enters from ICA to ECA through blunt nose flow divider, but in elastic model flow in ICA becomes so week and also a separation zone can be observed at non-divider side of ECA entrance. In solid model, flow moves like a wave that passes through CCA to ICA and ECA and no vortex can be observed. The velocity magnitude in the Mooney-Rivlin and the solid wall models are higher than the linear elastic model.

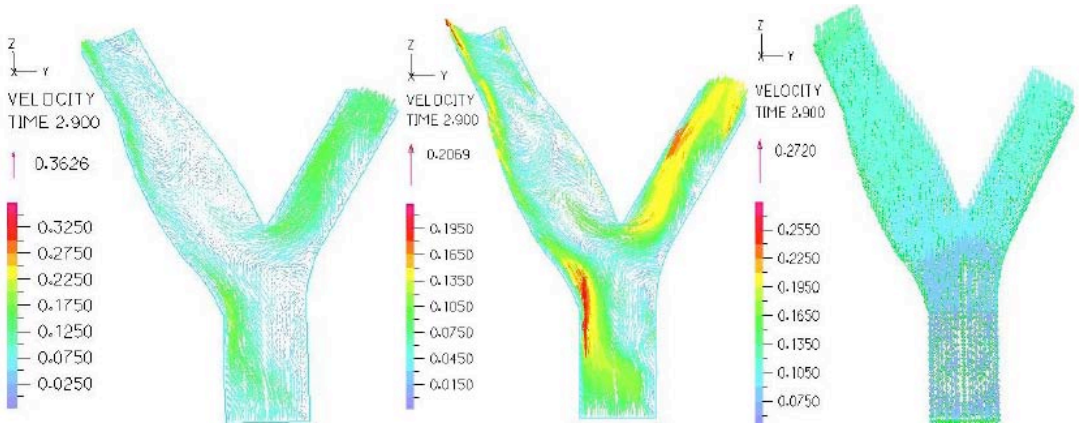

Figure14: Velocity vector plot at axial plane and end systole(t/t_p=2.90). From left to right: Mooney-Rivlin, linear elastic and solid models.

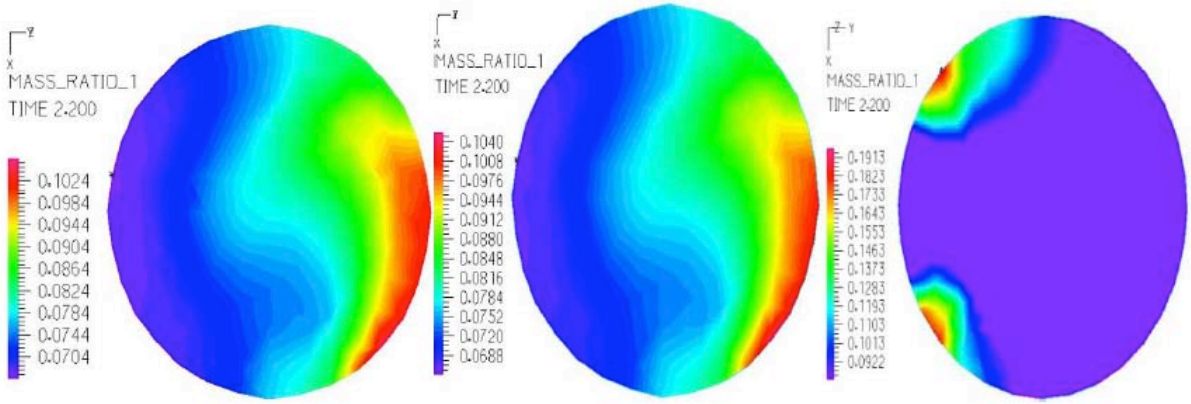

Figure15: Mass ratio band plot at ICA entrance and early systole (t/t_p=2.2). From left to right: Mooney-Rivlin, linear elastic and solid models.

Figure **14** is shown the velocity profile at axial cutting plane and end diastole. In the Mooney-Rivlin model, flow in ICA region is so week and enter to ECA through blunt nose flow divider. In the linear elastic model, one large vortex occupies most part of ICA and flow moves from ICA to ECA near blunt nose flow divider. In the solid wall model uniform flow is seen in all regions. But vortex and back flow are absent. The velocity magnitude in the linear elastic model is higher than the other models.

It can be concluded that except velocity magnitude, Mooney-Rivlin model and linear elastic model behave very similar to each other, but solid model is unable to predict secondary flow, vortexes, separation and back flow regions which is in contrast with helical flow phenomena in ICA. This model predicts a very uniform and unidirectional flow.

6.2. LDL Mass Ratio

The LDL concentration (or mass ratio) is a primitive symptom of LDL particle accumulation helps us diagnose areas that are face to atherosclerosis plaque formation. Therefore comparison between LDL accumulation, which obtained from result and clinical data can be a key to choose best wall model for large arteries like carotid bifurcation.

Figure **15** is shown the mass ratio at the entrance of internal carotid and early systole. The Mooney-Rivlin and the linear elastic models predict high-value LDL mass ratio at center towards divider wall and the other regions have the low value LDL mass ratio. The maximum values can be observed near divider wall. The solid wall model shows maximum values at anterior and posterior sides of non-divider wall and low values at the other regions.

Figure **16** is shown the mass ratio at the entrance of internal carotid and end systole. In this step all models show high LDL mass ratio through all of the cross section but the solid wall model predicts higher values (near twice) than the other models. The Mooney-Rivlin and the linear elastic models show a lower LDL mass ratio near center of cross section.

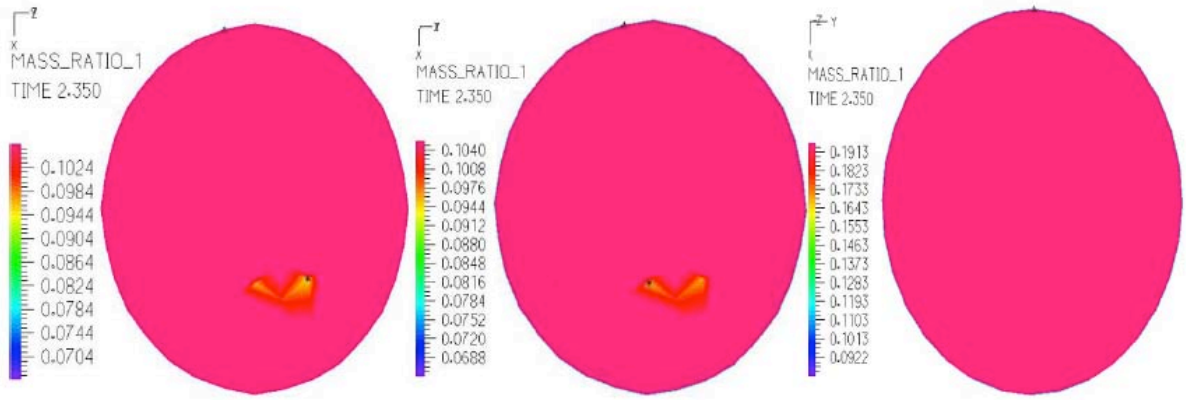

Figure 16: Mass ratio band plot at ICA entrance and end systole (t/t_p=2.35). From left to right: Mooney-Rivlin, linear elastic and solid models.

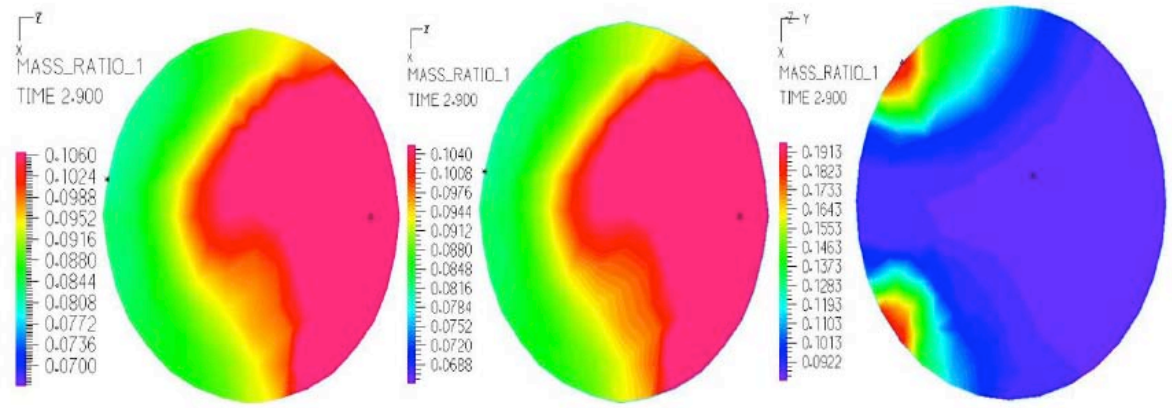

Figure 17: Mass ratio band plot at ICA entrance and end diastole (t/t_p=2.90). From left to right: Mooney-Rivlin, linear elastic and solid models.

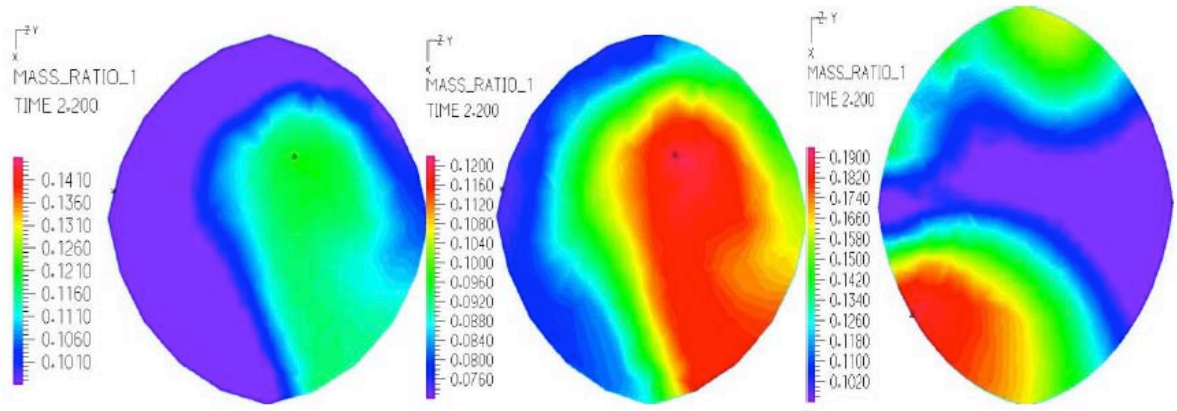

Figure 18: Mass ratio band plot at ICAsinus and early systole(t/t_p=2.2). From left to right: Mooney-Rivlin, linear elastic and solid models.

Figure **17** is shown the mass ratio at the entrance of internal carotid and end diastole. The Mooney-Rivlin and the linear elastic models predict high LDL mass ratio near the divider wall and center. Also the low LDL mass ratio is seen near the non-divider wall. The solid wall model shows very similar pattern to early systole (high LDL mass ratio regions become larger). In the solid model, the LDL mass ratio magnitude in high region is so higher than the other models.

As shown in figure **18**, for the Mooney-Rivlin and the linear elastic models the maximum LDL mass ratio values are seen at center and near divider wall at sinus region and early systole. In the linear elastic model

there is no evident border between low and high regions. In the solid model high and low LDL mass ratio values are observed at anterior side of non-divider wall and a region that extended from non-divider wall to divider wall through center line, respectively. Again in the solid model, the LDL mass ratio magnitude is so higher than the other models.

Figure **19** is shown the mass ratio at sinus region and end systole. The Mooney-Rivlin and the linear elastic models show high values at posterior region of the cross section and low values at anterior wall toward non-divider wall. But in the solid wall model a relative uniform mass ratio region can be seen in all over the cross section, which is higher than the other models prediction.

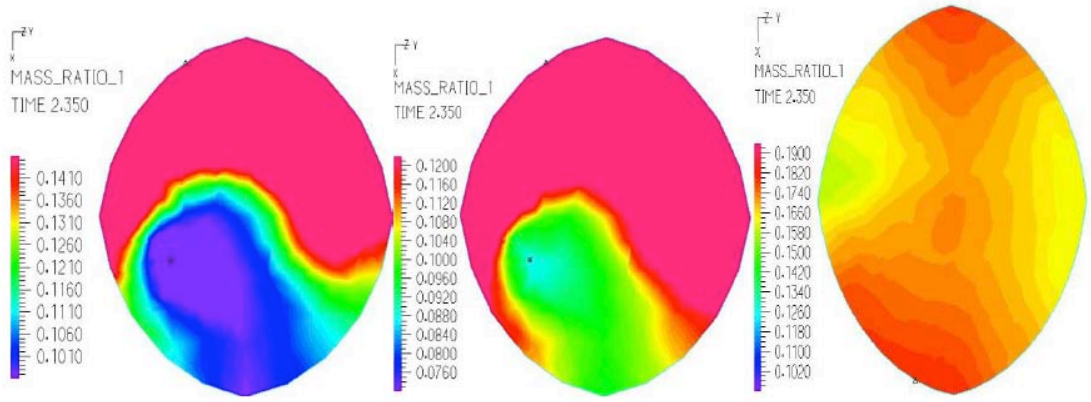

Figure 19: Mass ratio band plot at ICAsinus and end systole(t/t_p=2.35). From left to right: Mooney-Rivlin, linear elastic and solid models.

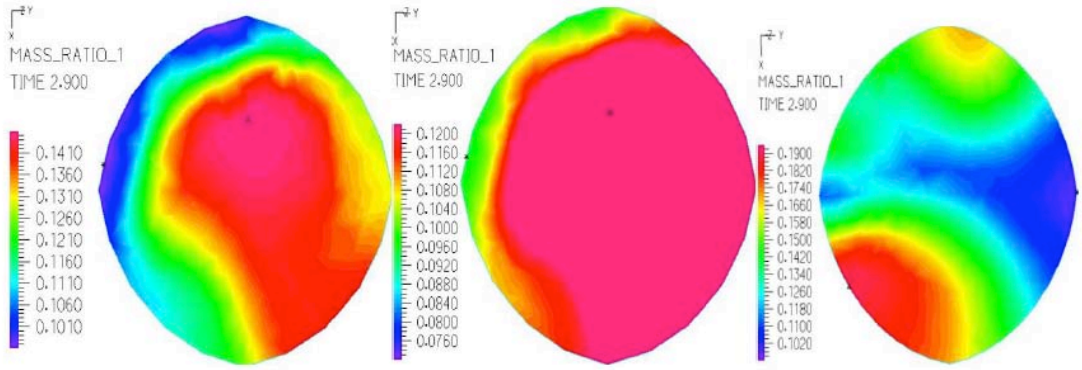

Figure 20: Mass ratio band plot at ICAsinus and end diastole(t/t_p=2.90). From left to right: Mooney-Rivlin, linear elastic and solid models.

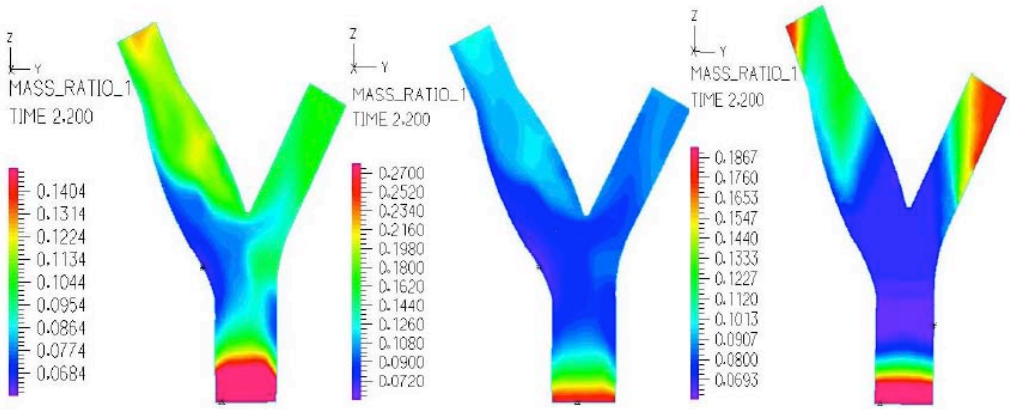

Figure 21: Mass ratio band plot at axial plane and early systole(t/t_p=2.2). From left to right: Mooney-Rivlin, linear elastic and solid models.

Figure **20** is shown the mass ratio at sinus region and end diastole. The Mooney-Rivlin and the linear elastic models predict high LDL mass ratio at center and anterior side of divider wall and low values at the posterior side of the non-divider wall. In the solid model the high LDL mass ratio exists at anterior side of non-divider wall and low values at divider wall. The Solid, Mooney-Rivlin and linear elastic model predict higher LDL mass ratio values respectively.

Figure **21** is shown the mass ratio at axial cutting plane and early systole. In Mooney-Rivlin and linear elastic models, maximum value of LDL mass ratio locates at the entrance of CCA and its minimum value exists near ICA and ECA non-divider wall entrance. In the solid wall model, the high LDL mass ratio value exists at CCA inlet and ICA and ECA outlets. The other regions have low values and the LDL mass ratio distribution is nearly symmetric in ICA and ECA.

Figure **22** is shown the mass ratio at axial cutting plane and end systole. In the Mooney-Rivlin and the linear elastic models, the high LDL mass ratio exists at ECA divider wall, ICA divider and non-divider wall. The lowest values can be observed at ICA outlet. In the solid model, all of the bifurcation regions have high values and the other regions have relatively low values. Also the linear elastic model shows the higher LDL mass ratio values than the other models.

Figure **23** is shown the mass ratio at axial cutting plane and end diastole. The Mooney-Rivlin and the linear elastic models show higher and lower the LDL mass ratio near the divider wall of sinus and the non-divider wall entrance of ICA respectively. In the solid model CCA and bifurcation regions have low and ICA and ECA outlet have high LDL mass ratio respectively. Also the linear elastic model predict higher LDL mass ratio than the other models.

6.3. Wall Shear Stress(WSS) and Wall Displacement in Sinus Region

Sinus region of ICA is the most prevalent to atherosclerosis plaque formation. In many researches low WSS introduced as an important factor of

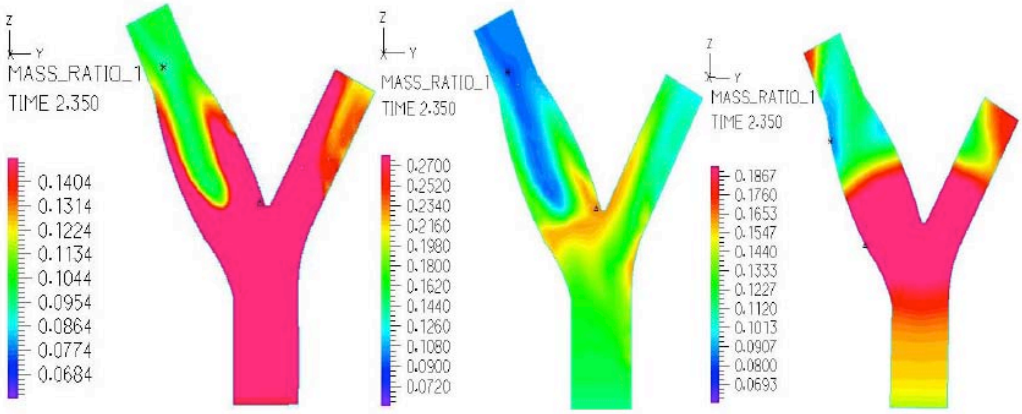

Figure 22: Mass ratio band plot at axial plane and end systole (t/t_p=2.35). From left to right: Mooney-Rivlin, linear elastic and solid models.

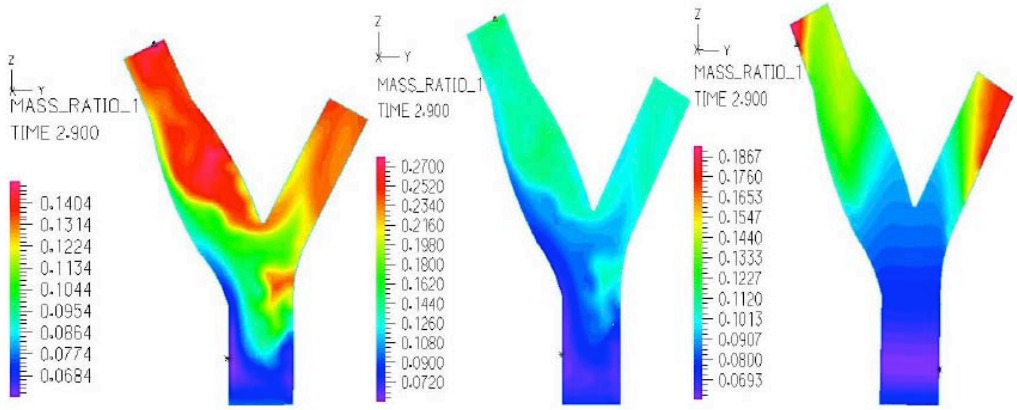

Figure 23: Mass ratio band plot at axial plane and end diastole (t/t_p=2.90). From left to right: Mooney-Rivlin, linear elastic and solid models.

atherosclerosis plaque formation. So WSS and wall displacement investigated in this area.

6.3.1. Wall Displacement

As shown in figure **24**, the Mooney-Rivlin (M-R) model predicts more displacement at both divider and non-divider walls rather than the linear elastic model. Also the solid model has no wall displacement. In all elastic models, non-divider wall displacement is more than divider wall displacement.

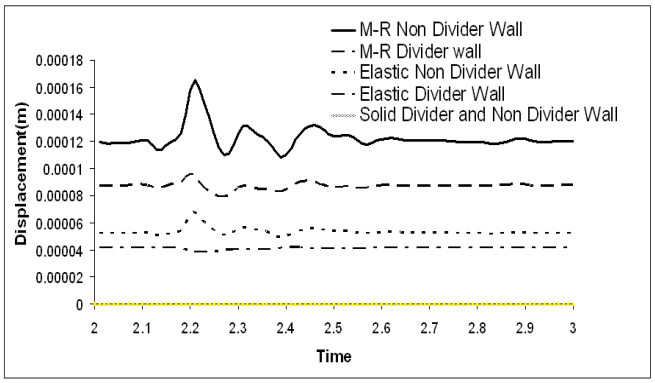

Figure 24: Sinus walls displacement.

6.3.2. XY-Wall Shear Stress

The XY-Wall shear stress is shown in figure **25**. At non-divider wall, the linear elastic model predicts the maximum value and the Mooney-Rivlin model has the second place. For divider wall, XY-WSS in linear elastic model is more than the Mooney-Rivlin model. Therefore the Mooney-Rivlin model predicts the lower WSS at sinus region than the linear elastic model. Also XY-WSS for the solid model is very smaller rather than the other models and is near zero for divider and non-divider walls.

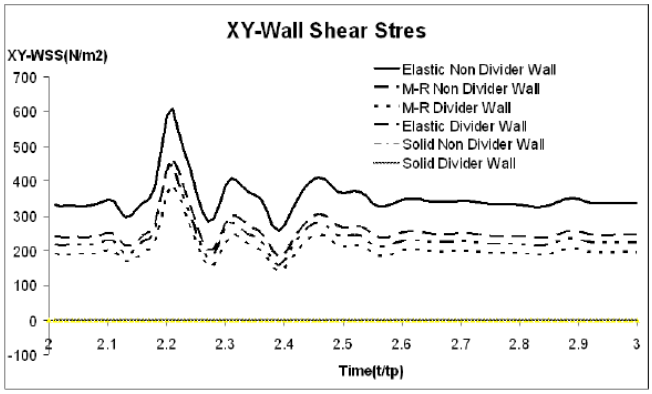

Figure 25: XY-WSS at sinus.

6.3.3. XZ-Wall Shear Stress

The XZ-Wall shear stress is shown in figure **26**. The Mooney-Rivlin (M-R) model predicts lower XZ-WSS component value at the divider wall rather than the linear elastic model. Also these phenomena can be seen at the non-divider wall. In the solid model XZ wall shear stress, has the lowest values at two sides of the sinus like XY-WSS.

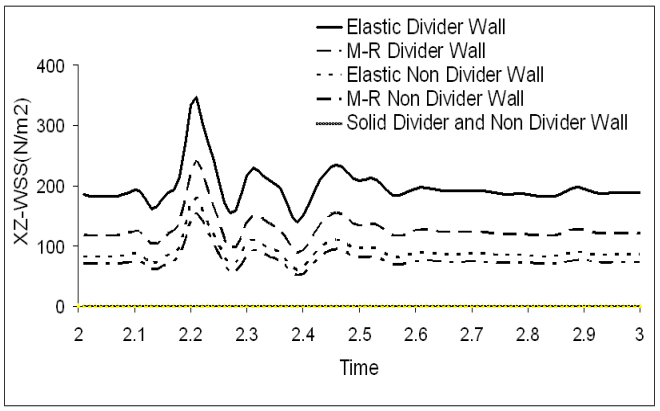

Figure 26: XZ-WSS at sinus.

6.3.4. YZ-Wall Shear Stress

The YZ-Wall shear stress is shown in figure **27**. The Mooney-Rivlin (M-R) model predicts higher values at divider and non-divider walls than the linear elastic model. At peak systole, in the Mooney-Rivlin model at divider and non-divider wall YZ-WSS is the same. It is important to note that in the linear elastic model at divider wall during the cardiac cycle, except in peak systole, YZ-WSS is negative. In the solid model, the YZ-WSS are very low and is nearly zero, which is similar to the other WSS components.

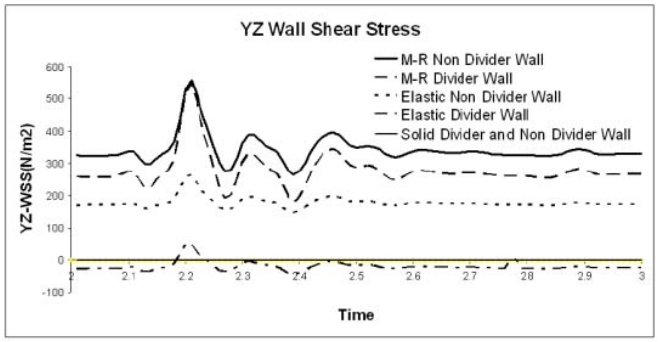

Figure 27: YZ-WSS at sinus.

CONCLUSION AND DISCUSSION

In this study, we investigate the wall elasticity effects on the blood flow and the wall motions. Blood modeled as Carreau and three wall model selected: (1) hyperelastic model (Mooney-Rivlin) (FSI analysis performed) (2) Linear elastic model (FSI analysis performed) and (3) Solid wall model.

Results show that the Mooney-Rivlin and the linear elastic models approximately predict very similar velocity patterns and values in all cross sections. But in the solid wall model vortexes are absent and the LDL mass transfer represents like a wave that initiates moving from CCA inlet and disperses to ICA and ECA through bifurcation. Also the linear elastic model and the Mooney-Rivlin model show similar LDL mass ratio distribution. Only the linear elastic model predicts the higher LDL mass ratio than the Mooney-Rivlin model. The Mooney-Rivlin and the linear elastic models just differ from each other at the absolute minimum and maximum of LDL mass ratio.

Also the Mooney-Rivlin model at the X-Y and the X-Z components at the divider and the non-divider walls predicts lower WSS values than the linear elastic model. This result for Y-Z component is vice versa. The solid wall model predicts very low values at both sides of sinus region, which is not confirmed by experimental results.

Based on this simulation, the wall and blood behavior are different in the solid and the linear elastic or Mooney-Rivlin models.

It seems for arteries like carotid bifurcation, which is located in heart vicinity, the solid wall model is not adequate. The Linear elastic and the Mooney-Rivlin (hyperelastic) models are very similar in flow field and the LDL mass transfer. In arterial wall simulation, the Mooney-Rivlin model predicts lower X-Y and X-Z WSS components in comparison to the linear elastic. The linear elastic model predicts lower Y-Z WSS than Mooney-Rivlin model.

There is not very important difference between the liner elastic and the rubber like material model results to predict the flow pattern and LDL mass transfer. But the Mooney-Rivlin model would be more accurate to simulate the wall behavior.

At the end, we report that the hyperelastic models (Mooney-Rivlin) are the best arterial wall model for large arteries like carotid bifurcation and also the linear wall elastic model is in the second place and shows more acceptable behavior in comparison with the solid wall model.

REFERENCE

[1] Khakpour S, Wan Abas WAB, AbdRazak NA and Abu Osman NA. Carotid atherosclerosis disease: A review of diagnosis, risk factors and simulations. Clinical Case Reports and Reviews 2016; 2(9): 537-550. https://doi.org/10.15761/CCRR.1000269

[2] Perktold K and Hilbert D. Numerical simulation of pulsatile flow in a carotid bifurcation model. Journal of Biomedical Engineering 1986; 8(3): 193-9. https://doi.org/10.1016/0141-5425(86)90083-X

[3] Marshall I, Zhao S, Papathanasopoulou P, Hoskins P and Yun XuX. MRI and CFD studies of pulsatile flow in healthy and stenosed carotid bifurcation models. Journal of Biomechanics 2004; 37(5): 679-87. https://doi.org/10.1016/j.jbiomech.2003.09.032

[4] Meagher S, Poepping TL and Ramnarine KV. Anatomical flow phantoms of the nonplanar carotid bifurcation, part II: experimental validation with Doppler ultrasound. Ultrasound in med and bio1 2007; 33(2): 303-10. https://doi.org/10.1016/j.ultrasmedbio.2006.08.004

[5] Moayeri MS and Zendehbudi GR. Effects of elastic property of the wall on flow characteristics through arterial stenosis. Journal of Biomechanics 2003; 36(4): 525-35. https://doi.org/10.1016/S0021-9290(02)00421-9

[6] Zhao SZ, Xu XY and Hughes AD. Blood flow and vessel mechanics in physiologically realistic model of a human carotid arterial bifurcation. Journal of Biomechanics 2000; 33(8): 975-84. https://doi.org/10.1016/S0021-9290(00)00043-9

[7] Stephanis CG, Mourmouras DE and Tsagadopoulos DG. Short communication on the elastic properties of arteries. Journal of Biomechanics 2003; 36(11): 1727-31. https://doi.org/10.1016/S0021-9290(03)00188-X

[8] Valencia A and Solis F. Blood flow dynamics and arterial wall interaction in a saccular aneurysm model of the basilar artery. Computers and Structures 2006; 84(21): 1326-37. https://doi.org/10.1016/j.compstruc.2006.03.008

[9] Kural MH, Cai M, Tang D, Gwyther T, Zheng J, *et al*. Planar biaxial characterization of diseased human coronary and carotid arteries for computational modeling. Journal of Biomechanics 2012; 45(5): 790-98. https://doi.org/10.1016/j.jbiomech.2011.11.019

[10] Yang C, Canton G, Yuan C, Ferguson M, Hatsukami TS, *et al*. Advanced human carotid plaque progression correlates positively with flow shear stress using follow-up scan data: An in vivo MRI multi-patient 3D FSI study. Journal of Biomechanics 2010; 43(13): 2530-38. https://doi.org/10.1016/j.jbiomech.2010.05.018

[11] Stroud JS, Berger SA and Saloner D. Infuence of stenosis morphology on flow through severelystenotic vessels: implications for plaque rupture. J Biomech 2000; 33(4): 443-55. https://doi.org/10.1016/S0021-9290(99)00207-9

[12] Perktold K, Peter RO, Resch M and Langs G. Pulsatile non-newtonian blood flow in three-dimensional carotid bifurcation models: a numerical study of flow phenomena under different bifurcation angles. Journal of Biomedical Engineering1991; 3(6): 507-15. https://doi.org/10.1016/0141-5425(91)90100-L

[13] Gijsen FJH, van de Vosse FN and Janssen JD. The influence of the non-Newtonian properties of blood on the flow in large arteries: steady flow in a carotid bifurcation model. Journal of Biomechanics1999; 32(6): 601-8. https://doi.org/10.1016/S0021-9290(99)00015-9

[14] Razavi A, Shirani E and Sadeghi M. Numerical simulation of blood pulsatile flow in a stenosed carotid artery using different rheological models. Journal of Biomechanics 2011; 44(11): 2021-30. https://doi.org/10.1016/j.jbiomech.2011.04.023

[15] Jou LD and Saloner D. A numerical study of magnetic resonance images of pulsatile flow in a two dimensional carotid bifurcation: A numerical study of MR images. Medical Engineering and Physics 1998; 20(9): 643-52. https://doi.org/10.1016/S1350-4533(98)00075-7

[16] Perktold K, Resch M and Peter RO. Three-dimensional numerical analysis of pulsatile flow and wall shear stress in

the carotid artery bifurcation. Biomechanics 1991; 24(6): 409-20.
https://doi.org/10.1016/0021-9290(91)90029-M

[17] Polak JP. Peripheral Vascular Sonography. Second ed. Philadelphia: Lippincott Williams and Wilkins 2004.

[18] Nicolosi RJ and Lawton CWT. A.Vitamin E reduces plasma low density lipoprotein cholesterol, LDL oxidation, and early aortic atherosclerosis compared with black tea in hypercholesterolemic hamsters. Nutrition Research1999; 19(8): 1201-14.
https://doi.org/10.1016/S0271-5317(99)00081-0

[19] Vasankari T, Ahotupa M, Toikka J, Mikkola J, Irjala K, Pasanen P, *et al.* Oxidized LDL and thickness of carotid in tima-media are associated with coronary atherosclerosis in middle-aged men: lower levels of oxidized LDL with statin therapy. Atherosclerosis 2001; 155(2): 403-12.
https://doi.org/10.1016/S0021-9150(00)00573-6

[20] Hu B, Li D, Sawamura T and Mehta JL. Oxidized LDL through LOX-1 modulates LDL-receptor expression in human coronary artery endothelial cells. Biochemical and Biophysical Research Communications 2003; 307(4): 1008-12.
https://doi.org/10.1016/S0006-291X(03)01295-6

[21] Bharadvaj BK, Mabon RF and Giddens DP. Steady flow in a model of the human carotid bifurcation. Part I—Flow visualization. Journal of Biomechanics1982; 15(5): 349-62.
https://doi.org/10.1016/0021-9290(82)90057-4

[22] Ghassemi M, Shahidian A, Ahmadi G and Hamian S. A new effective thermal conductivity model for a bio-nanofluid (blood with nanoparticle Al2o3). Journal of International communication in Heat and Mass transfer 2010; 37(7): 929-34.
https://doi.org/10.1016/j.icheatmasstransfer.2010.04.010

[23] Tank DW, Fredericks W, Barak L and Webb W. Electric Field-induced Redistribution and Post field Relaxation of low density lipoprotein. The journal of cell biology1985; 101(1): 148-57.
https://doi.org/10.1083/jcb.101.1.148

[24] Habibi MR, Ghassemi M and Shahidian A. Investigation of biomagnetic fluid flow under nonuniform magnetic fields. Nanoscale and Microscale Thermo physical Engineering 2012; 16(1): 64-77.
https://doi.org/10.1080/15567265.2011.645998

[25] Karimi R, Zhu T, Bouma B, Kaazempur M and ofrad M. Estimation of nonlinear mechanical properties of vascular tissues via Elastography. Cardiovasc Eng 2008; 8(4): 191-202.
https://doi.org/10.1007/s10558-008-9061-0

[26] Tang D, Yang C, Walker H, Kobayashi S and Ku DN. Simulating cyclic artery compression using a 3D unsteady model with fluid–structure interactions. Computers and Structures 2002; 80(20-21): 1651-65.
https://doi.org/10.1016/S0045-7949(02)00111-6

[27] Sui B, Gao P, Lin Y, Qin H, Liu L and Liu G. Non invasive determination of spatial distribution and temporal gradient of wall shear stress at common carotid artery. Journal of Biomechanics 2008; 41(14): 3024-30.
https://doi.org/10.1016/j.jbiomech.2008.07.026

Received on 28-05-2017 Accepted on 23-08-2017 Published on 16-12-2017

DOI: http://dx.doi.org/10.12974/2311-8792.2017.05.3